applied sciences

MDPI

*Article*

# Model Test Study on a Shield Tunnel Adjacent to Pile in the Sub-Clay of a Coastal Area

**Xuan Guo [1,2], Zhitong Li [3,*], Xiaoli Zhang [4] and Mengjun Pu [2]**

1 Key Laboratory of Urban Underground Engineering of Ministry of Education, Beijing Jiaotong University, Beijing 100044, China; xguo@bjtu.edu.cn
2 School of Civil Engineering, Beijing Jiaotong University, Beijing 100044, China; pumengjun21@163.com
3 Architecture Department, Shijiazhuang Institute of Railway Technology, Shijiazhuang 050041, China
4 China Railway Fifth Survey and Design Institute Group Co., Ltd., Beijing 102600, China; zhangxiaoli_t5y@163.com
* Correspondence: lizhitong_sirt@163.com; Tel.: +86-132-3046-9930

**Abstract:** In this study, a model test system of shield driving adjacent to pile is realized to study the response of surrounding rock and pile induced by an advanced shield tunnel in silty clay layer in a coastal area. The function of automatic pushing and the synchronous grouting of the shield were partially simulated. Similar materials of lining, soft rock and pile, were developed. A total of 33 sets of orthogonal model tests were designed to study the progressive failure caused by excavation in silty clay and the change in stratum displacement and soil pressure; the displacement and internal force response of the pile were also analyzed. The following conclusions can be given: (1) the best grouting filling coefficient range of the shield test for the case study is 1.4 to 1.6; (2) the fitting of the experimental data to obtain the settlement through the width parameter suggests that the *K* value of the surrounding rock is decreased by 0.075 at least, and the *K* value increases with the increase in pile-tunnel distance and decreases with the increase in pile depth; and (3) the weak surrounding rock in the tunnel system can be divided into five zones according to the displacement and pressure change in soft surrounding rock and the pile response in the case study. The key condition control factor was also determined.

**Keywords:** shield tunnel; sub-clay grouting; pile; model test



**Citation:** Guo, X.; Li, Z.; Zhang, X.; Pu, M. Model Test Study on a Shield Tunnel Adjacent to Pile in the Sub-Clay of a Coastal Area. *Appl. Sci.* **2022**, *12*, 7718. https://doi.org/10.3390/app12157718

Academic Editor: Daniel Dias

Received: 9 June 2022
Accepted: 28 July 2022
Published: 31 July 2022



## 1. Introduction

The geological conditions of silty clay in coastal areas are complex. The geological characteristics of coastal silty clay vary between cohesive soil and sandy soil. The deformation mechanism is more complex under the disturbance of shield construction. In addition, the permeability and the stability of the formation are poor, and the disturbance degree of the surrounding rock is significant. Under these geological conditions, retaining the effect of pile is important and its mechanical properties deserve attention. At the same time, the effect of grouting on the soil with the pile foundation is also a cause for concern.

Through model tests and theoretical analysis, scholars have carried out a significant amount of research on the interaction between the surrounding rock-pile caused by shield construction, providing some beneficial insights. The scale model test was carried out on the Φ800 mm earth pressure balance shield test system to study the influence of shield on sand pebbles and sand strata [1]. Hergarden [2] applied the centrifugal model test to determine the influence of tunnel excavation on the end bearing of the pile; the pile was greatly affected by the spacing of the pile-tunnel, which was less than 0.25*D* (*D* is the diameter of the tunnel). An increase in soil loss will cause an increase in the vertical amount of pile settlement if the spacing of the pile-tunnel is in the 0.25*D*–1*D* range. This influence will be relatively small if the spacing of the pile-tunnel is greater than 2*D*. Using the indoor model test of tunnel excavation migration and adjacent pile caused by the variation in the bearing capacity of pile, Ghahremannejad [3] concluded that the maximum bending moment of pile tunnel spacing is 1.5*D*, which increases with an increase in soil loss.

According to an analysis of the line selection of the English Channel and the relationship between the settlement of the pile and the settlement of the surface, Selemeta [4] partitioned the surrounding rocks of the tunnel as shown in Figure 1, with *R* as the ratio of pile settlement to surface subsidence. The settlement of the layer is larger than that of the pile in zone A, and zone B is close to it, while zone C shows that the settlement of the pile is less than the soil settlement.

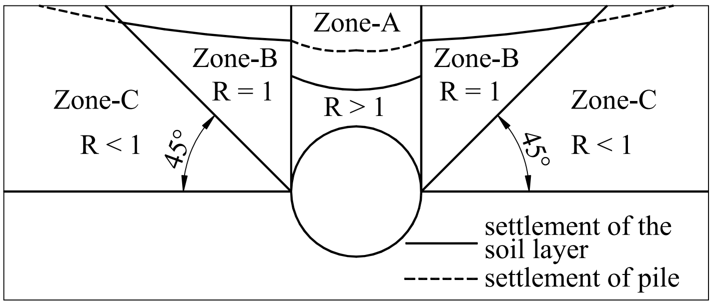


**Figure 1.** Surrounding rock zone division by shield.

The present study is focused on the soft surrounding rock of shielding and the settlement of sandy pebble strata. Studies on the weak strata temperature and the earth pressure of silty clay are limited, therefore the influence of temperature on soil properties were considered [5,6]. There are a few cases in which the model test method has been used to study the shield effect on the displacement of pile, the earth pressure and the displacement of pile and the internal force response [7]. These studies are of great significance for the design and construction of tunnel and underground engineering in coastal areas in order to determine the law of strata disturbance and the response of pile.

The soil pressure distribution, deformation and failure law, in addition to different positions of pile internal force and the displacement of the response caused by shielded pile, are studied for the silty clay strata (according to the surrounding rock classification V and VI of railway tunnels [8]). This study provides a preliminary reference for understanding the soil deformation and pressure distribution of shield tunneling in silty-clay layers and the formation of the shield-pile system within the initial area of the layers. An analysis of the key digging factors is given.

## 2. Design of Model Test System Crossing Existing Piles by Shielding

### *2.1. Model Test System of Crossing Existing Piles by Shielding*

A plane strain shield tunneling model test system was designed to realize automatic pushing and tail grouting. It is mainly composed of four parts: the test platform, the shield grouting module, the loading module and the monitoring module (Figure 2).

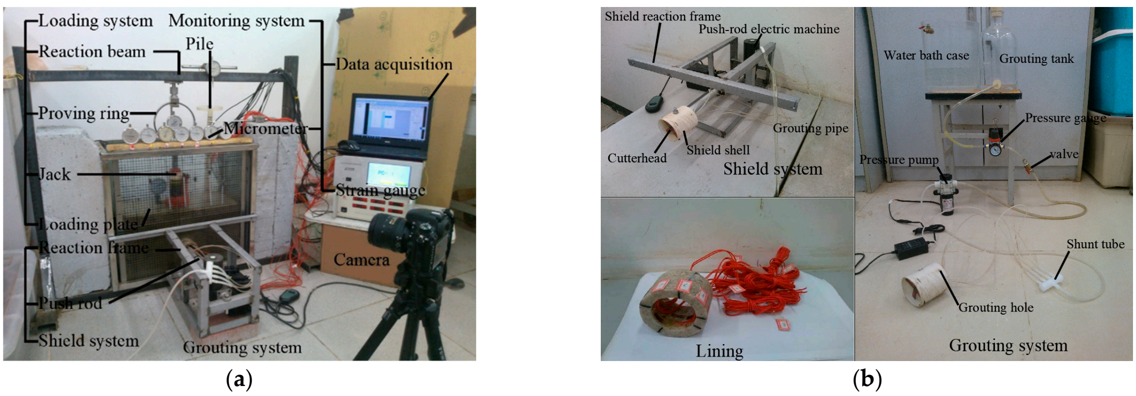


**Figure 2.** The model test system (**a**) the overall test device; (**b**) part of test device.

The size of the model chamber is 520 mm × 200 mm × 520 mm (length × width × height). In order to reduce the boundary effect, the experiment adopts the transparent tempered $SiO_2$ glass material; 5 cm thickness can ensure that the surface deformation is less than 0.2 mm. The simulation prototype is the shield engineering project of Tianjin Metro Line 1. The diameter of the circular section is 6390 mm, the geometric similarity ratio is 1:100, and the circular hole with 80 mm diameter is opened in the front part of the chamber with a peripheral angle steel reinforcement and an outer alloy steel support frame. The test system is shown in Figure 2.

The shield module consists of a welded steel frame and can provide a 6 kN thrust range of the putter composition, and the pushing speed is 1 mm/s, which can realize the automatic push driving. The grouting module is mainly composed of a diaphragm pressure pump which can provide 2 kPa grouting pressure. The preparation of slurry for the modified Vaseline material has good cement and mobility ability after heating and the grouting rings have a solid-state solid and similar soil formation. The loading system consists of the force ring and the range 2000 kg hydraulic jack, which completes the initial consolidation of the layers at each stage of the each loading of 60 kN, corresponding to the surface applied surface force of 1 kPa. The test monitoring modules are composed of contact type (dial gauge, earth pressure cell, strain gauge) and non-contact observation (camera, 1 cm grid, PIV software, etc.).

The main observation index: load value, soil surface subsidence, soil displacement, soil stress value, bending moment and displacement, pile failure process. The earth pressure and layered settlement monitoring systems are shown in Figures 3 and 4. The micrometer accuracy of the test system is 0.001 mm, and the corresponding actual displacement accuracy is 0.1 mm, which meets the test requirements.

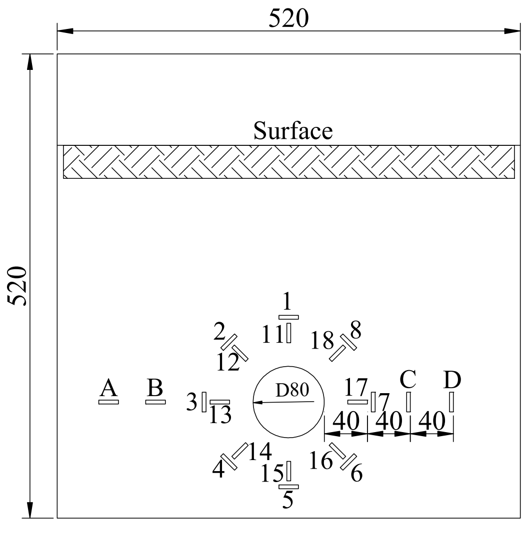


**Figure 3.** The layout of pressure-cell (mm). Note: Radial pressure monitoring 1~8, C, D; Circumferential pressure monitoring 11~18, A, B.

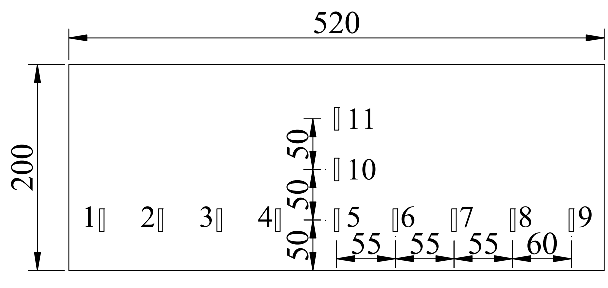


**Figure 4.** The layout of displacement meter (mm). Note: Surface lateral subsidence monitoring 1~9; Surface Longitudinal Subsidence Monitoring 5, 10, 11.

### 2.2. Design of Test Materials

#### 2.2.1. Equivalent Materials

The actual soil is a typical silty clay layer in the coastal area, and the model material is selected according to the classification of surrounding rock for a railway tunnel of grade V and VI. The geometric similarity constant $C_l = 100$, the bulk density similar constant $C_\gamma = 1$, according to the similarity of the two mechanical behaviors and phenomena, the following similarity law indicators can be obtained:

$$C_\varepsilon = C_\mu = C_\varphi = 1 \quad (1)$$

$$C_\sigma = C_E = C_c = 100 \quad (2)$$

The results show that the clean sand, 200 mesh barite powder and Vaseline were the appropriate main simulation materials. After repeated tri-axial and shear tests, a mass ratio of 8:3:1 with a similar relationship was determined. The stress–strain relationship at different confining pressures is presented in Figure 5. The deformation modulus $E$ = 13.1 MPa and the relationship between shear stress–strain is shown in Figure 6. The relationship between shear strength and vertical pressure is shown in Figure 7. The cohesive force $C$ = 0.375 kPa, the internal friction angle $\varphi$ = 31.35°; the physical-mechanical parameters of actual and model for surrounding rock are shown in Table 1. The deformation modulus, cohesion and internal friction angle presented the similar relationship to the railway tunnel surrounding rock of V, VI.

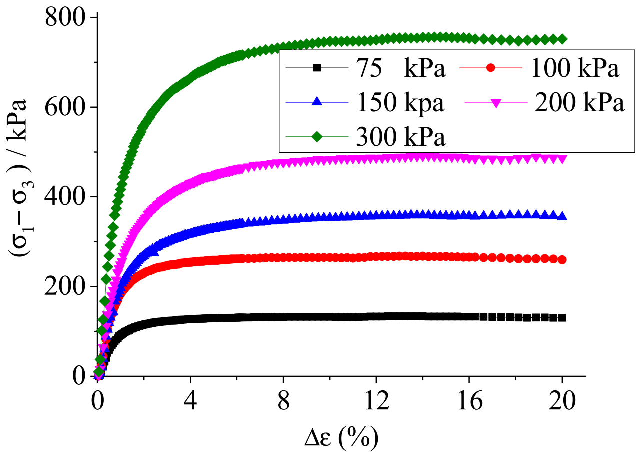


**Figure 5.** The stress–strain relation at different confining pressure.

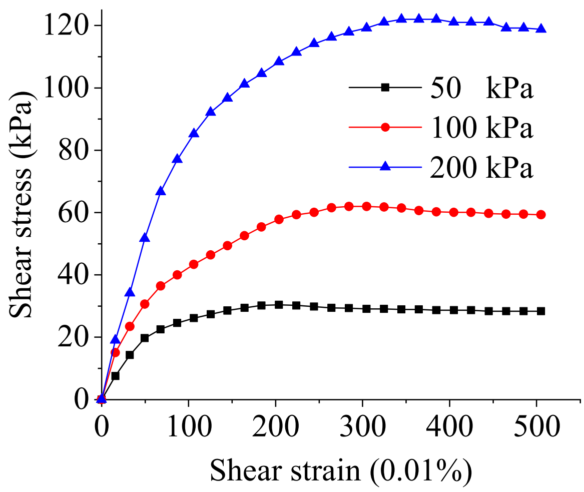


**Figure 6.** Shear stress–strain relations.

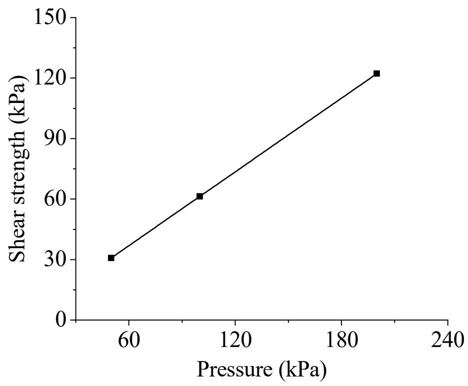


**Figure 7.** Shear strength-pressure relationship.

**Table 1.** Physical-mechanical parameters of prototype and model for surrounding layers.

| Grade | Bulk Density $\gamma$/(kN/m$^3$) | Deformation Modulus *E*/MPa | Cohesion *c*/kPa | Internal Friction Angle $\varphi$/° |
|---|---|---|---|---|
| V | 17~20 | 1000~2000 | 50~200 | 40~50 |
| VI | 15~17 | <1000 | <100 | 30~40 |
| Similar material | 20.6 | 13.1 | 0.375 | 31.35 |

2.2.2. Equivalent Lining

In order to develop similar material to the lining model test, paraffin wax, clean quartz sand and steel fiber were selected as the suitable main simulation materials. The material coefficients are shown in Table 2.

**Table 2.** Proportioning table of model material.

| Test Group | Paraffin Wax (g) | Quartz Sand (g) | Steel Fiber (g) | Scale |
|---|---|---|---|---|
| 1 | 150 | 0 | 0 | 1:-:- |
| 2 | 80 | 160 | 0 | 1:2:- |
| 3 | 60 | 240 | 0 | 1:4:- |
| 4 | 50 | 300 | 0 | 1:6:- |
| 5 | 40 | 360 | 0 | 1:8:- |
| 6 (steel-1) | 60 | 240 | 4 | 15:60:1 |
| 7 (steel-2) | 45 | 270 | 3 | 15:90:1 |
| 8 (steel-3) | 30 | 240 | 2 | 15:120:1 |

Tri-axial tests were conducted. The elastic modulus and fracture angle of the test specimens were detected. The vertical strain gauges were pasted on the surface of the specimen for monitoring. The Poisson's ratio, paraffin, quartz sand content and the elastic modulus relationship was obtained in Figure 8. According to the intersection point of the two curves, the physical and mechanical parameters of different proportions of test pieces are shown in Table 3. The mass ratio of the similarity relationship of the lining material was determined to be 15:90:1. From the physical and mechanical parameters of the prototype and model lining of Table 4, it can be seen that the material bulk density, elastic modulus and Poisson's ratio have a similar relationship.

**Table 3.** The physical and mechanical parameters of specimens with different proportions.

| Serial Number | 1 | 2 | 3 | 4 | 5 | 6 | 7 | 8 |
|---|---|---|---|---|---|---|---|---|
| weight (*g*) | 105.3 | 145.6 | 168.7 | 189.1 | 206.6 | 232.9 | 242.7 | 254.1 |
| bulk density (kN/m$^3$) | 10.4 | 14.5 | 16.8 | 18.8 | 20.6 | 23.2 | 24.2 | 25.3 |
| Poisson ratio | 0.45 | 0.35 | 0.35 | 0.34 | 0.34 | 0.33 | 0.33 | 0.32 |
| *E* (MPa) | 79.4 | 105.4 | 190.3 | 250.3 | 275.8 | 262.3 | 303.6 | 330.2 |
| Rupture angle (°) | — | — | 32 | 36 | 40 | 39 | 42 | 46 |

**Table 4.** Physical-mechanical parameters of prototype and model lining.

| Lining | Bulk Density $\gamma$/kN/m$^3$ | Deformation Modulus *E*/GPa | Poisson Ratio $\mu$ |
|---|---|---|---|
| Prototype material | 24–27 | 20–35 | 0.2–0.35 |
| modeling material | 24.2 | 0.295 | 0.33 |

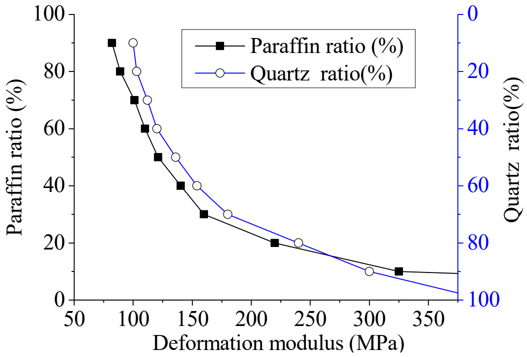


**Figure 8.** The relationship of E and material.

Bending deformation is an important control parameter of the lining safety. According to the similarity principle of bending deformation [9–11], the similar lining thickness hm was determined, and the lining structure was equivalent to the thin plate, where the thickness is $h$, the orthogonal coordinate $x$-$y$ of the cross section, the uniform force $q$ was applied, and the deflection of the plate satisfies the following equation.

$$\frac{\partial^4 \omega}{\partial x^4} + 2\frac{\partial^4 \omega}{\partial x^2 \partial y^2} + \frac{\partial^4 \omega}{\partial y^4} = \frac{q}{K} \tag{3}$$

$$K = \frac{Eh^3}{12(1-\mu^2)} \tag{4}$$

where $K$ is the bending stiffness, $E$ is Young's modulus, and $\mu$ is the Poisson's ratio.

The geometric similarity scale of the model device was set to $\alpha_l = 1/n$, then the model structure and the prototype structure met the Formula (3), to obtain the following similar criteria.

$$n^3 \frac{h_m^3}{h_p^3} = \frac{E_P(1-\mu_m^2)}{E_m(1-\mu_P^2)} \tag{5}$$

The formula for the thickness $h_m$ of the lining model was obtained:

$$h_m = \frac{h_P}{n}\left[\frac{E_P}{E_m}\frac{(1-\mu_m^2)}{\left(1-\mu_p^2\right)}\right]^{1/3} = \frac{0.35}{100}\left[\frac{28.5}{0.295}\frac{(1-0.33^2)}{(1-0.3^2)}\right]^{1/3} = 0.016m \tag{6}$$

### 2.2.3. Pile Model

The strain gauge measuring range of 1 με~20,000 με met the precision requirement conditions before reaching the loading limit. A PVC pipe with a diameter of 75 mm was designed and manufactured for the pile simulation test. The physical and mechanical parameters of pile are shown in Table 5; it basically had a similar relationship.

**Table 5.** Physical and mechanical parameters of prototype and model pile materials.

| Pile | Bulk Density $\gamma$/kN/m$^3$ | Deformation Modulus *E*/GPa | Poisson Ratio $\mu$ |
|---|---|---|---|
| Prototype material | 25 | 30 | 0.2 |
| modeling material | 13.5–14 | 0.2–0.4 | 0.33 |

The diameter of the prototype pile was 500 mm of concrete C30. The diameter of the test model was 18 mm, and the thickness of the pipe wall was 2 mm. According to the principle of equivalent stiffness, the basic similarity condition was satisfied.

$$E_P I_P \approx 100^4 E_M I_M \tag{7}$$

where:

$E_p$—Elastic modulus of prototype pile
$I_p$—Inertia moment of prototype pile
$E_M$—Elastic modulus of model pile
$I_M$—Inertia moment of model pile

## 3. Experiment Plan

To simulate the construction process of shield Metro in the silty clay layer, the displacement, internal force and collapse failure of the soil layer and the grouting parameters were studied. According to the different pile-tunnel positions with different coverage ratios ($H/D$ = 1, 2, 3) in Figure 9, the 27 groups of orthogonal schemes are designed in Table 6. The stress and deformation laws of weak surrounding rock and pile were studied, and the division of surrounding rock was carried out.

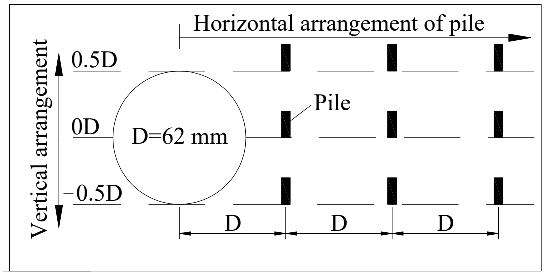


**Figure 9.** Position distribution of pile and tunnel.

**Table 6.** Orthogonal test schemes of pile model test.

| Test Group | Cover Span Ratio ($H/D$) | Vertical Position of Pile Bottom | Lateral Distance between Pile and Tunnel |
|---|---|---|---|
| | 1 | 0.5$D$ | 1$D$ |
| 1–27 | 2 | 0$D$ | 2$D$ |
| | 3 | −0.5$D$ | 3$D$ |

The orthogonal test mainly involved three parts: Excavation without support, excavation with support design, excavation with support through the pile, which were shown in Figure 10. The test process was divided into three main stages: The model soil layered filling stage, the monitoring equipment and the structure installation-commissioning stage, the dynamic excavation and real-time monitoring stage. The detailed steps were as follows:

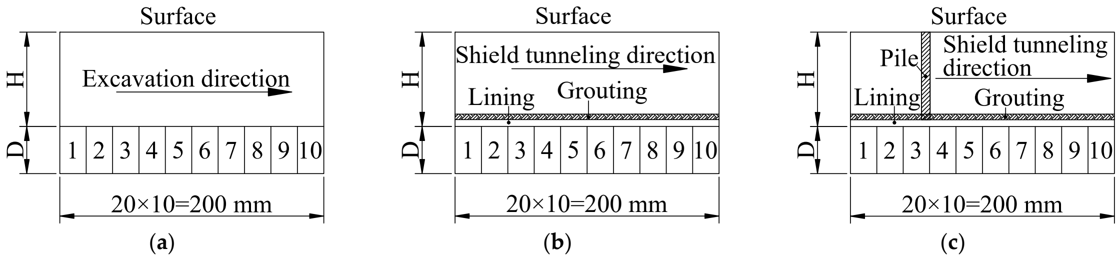


**Figure 10.** Excavation step of different work conditions: (**a**) Excavation without support; (**b**) Excavation with support design; (**c**) Excavation with support through the pile. The numbers 1, 2, 3 . . . means the number of construction steps or rings of excavation.

For model layers preparation, the mixed soils consolidated left for days until its basic parameters were calibrated equal to the prototype. The experiment was a success or not depended on the model layers, so it was necessary to strictly control the similarity parameters of the model test. In accordance with the thickness of each layer, 7 cm layers were filled, the jack and the loading plate were used to complete the consolidation, and samples were taken with a ring knife to test the compactness according to the standard of gravity, so as to ensure the filling quality. For model layers preparation, the mixed soils and left consolidations for days until its basic parameters were calibrated equal to the prototype. The experiment was a success or not depended on the model layers, so it was necessary to strictly control the similarity parameters of the model test. In accordance with the thickness of each layer, 7 cm layers were filled, the jack and the loading plate were used to complete the consolidation, and samples were taken with a ring knife to test the compactness according to the standard of gravity, so as to ensure the filling quality.

Model soil was filled to the measuring point position and the monitoring equipment and measuring point were arranged. It was left standing for 48 h after completion to ensure the similar soil reached a stable state. The monitoring devices were equipped after debugging and precision calibration to ensure data accuracy.

Excavation process: First, the shield pushing controller was started, then turned to full section jacking with a speed 1 mm/s, with the footage of 2 cm per ring, and digging shovel was used to clean out of the ejected soil in time. At the same time, the pressure pump was started to grout the liquid slurry evenly according to the grouting volume. After each ring of excavation and support was completed, it was allowed to stand for more than 20 min, so that the slurry solidified and the surrounding rock was fully deformed. After the reading of the monitor was stable, the next cycle of excavation was carried out, and the macro response of the surrounding rock and pile around the tunnel was dynamically recorded in real time. The whole process of video recording was convenient for later PIV software processing and observation of the displacement field.

The test observation contents mainly include the loading amount, surface settlement, soil stress value, displacement field, soil damage zone, pile internal force, pile top displacement, and the macro response of the whole process of the system.

## 4. Test Results

### 4.1. Excavation Failure

When the cover span ratio of $H/D = 1$, full section jacking without support was seen and the progressive failure occurred when excavation to the fifth ring. This process can be divided into four stages: the formation of a transient arch, large deformation cracking, slag falling from the tunnel top, and the collapse failure stage. During collapse and destruction, the turbulent characteristics of the soil particles were obvious and the observations were unstable, and therefore difficult to refine. Figure 11 shows the vector diagram of soil and the cloud diagram of the displacement field in the first three stages. The "funnel" shaped particle flow migration area of soil to the tunnel was obvious, and the vault settlement reached the maximum.

The test results were shown in Figures 12 and 13 when the coverage span ratio of $H/D = 2$ and 3. Uneven convergence and large deformation damage occurred around the tunnel, and the deformation of the arch crown was the largest, which were 5.08 mm and 4.55 mm, respectively. The test showed that there were two forms of failure: collapse and large deformation, in the unsupported excavation of the silty clay layer; therefore, it cannot be classified as self-stable.

Combined with the experimental observation and monitoring data, when $H/D = 1$, there was no stable soil arch formed, and the overlying soil pressure completely provided the vertical surrounding rock pressure. When $H/D = 2$, soil arching occurred, and it was considered an ultra-shallow buried tunnel when $H/D \leq 1$. When $H/D = 5$, there was a settlement and isolation area on the arch crown, and there was no settlement on the surface;

that is, a stable soil arch was formed from the arch crown to the surface, dissipating the soil settlement. It was considered that the tunnel achieved a deeply buried state at this time.

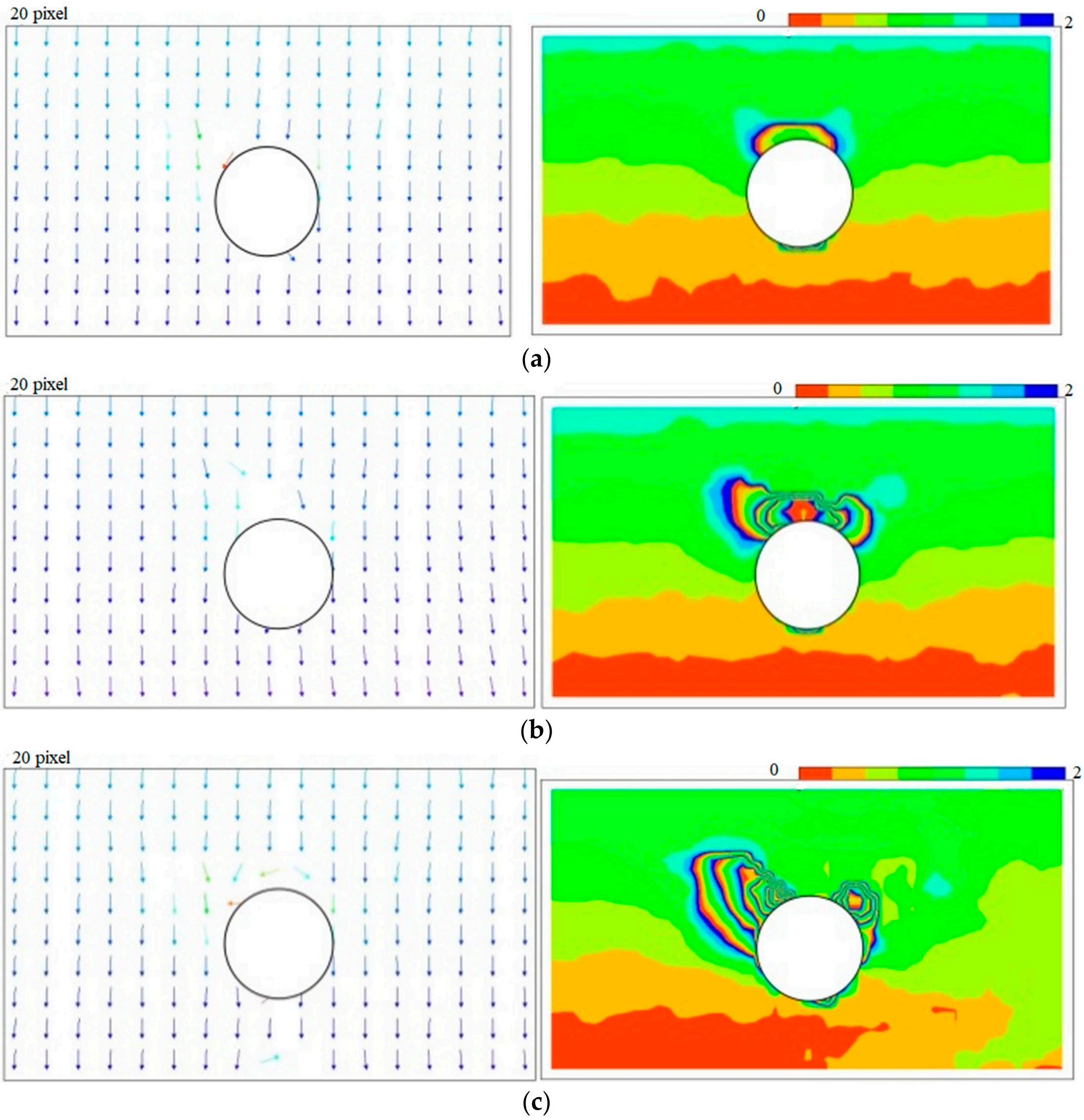


**Figure 11.** PIV vector diagram and contour of displacement: (**a**) Transient arch forming stage; (**b**) Large deformation-fracture stage; (**c**) Roof block falling stage.

**Figure 12.** Final state when $H/D = 2$.

**Figure 13.** Final state when $H/D = 3$.

### 4.2. Surface Deformation

The gap caused by shield tail prolapse was the main cause of surface deformation, and slurry filling was the main means of controlling surface deformation. According to the following formula, the free space and similar gap can be calculated as follows:

$$V_{gap} = \pi\left[R^2 - (R-d)^2\right] \cdot L = 3.14 \times \left[4^2 - (4-0.2)^2\right] \times 2 = 9.8\left(\text{cm}^3\right) \tag{8}$$

where: $V$ is the volume of gap; $R$ is the radius of the shield; $d$ is the thickness of the shield; $L$ is the movement distance.

The filling coefficient of the grouting was stipulated 1.4~2.5 in the code of the specification for shield construction of Metro Tunnel Engineering (STB/DQ-010001-2007). Considering the silty clay characteristics of the surrounding layers in this test, the grouting filling coefficient of 1.2, 1.4, 1.6 and 1.8 were selected to analyze the law of ground settlement and the surface sedimentation when $H/D = 1$.

When the grouting filling coefficient changes: 1.2→1.4→1.6→1.8, the displacement change law of measuring points 1–5 during the shield process is given in Figure 14 and the maximum surface settlement is −0.985→−0.422→−0.213→0.186 mm. The contours show that when the grouting filling coefficient reached 1.6, there was a certain degree of uplift in the soil layers, and when it reached 1.8, the surface uplift occurred.

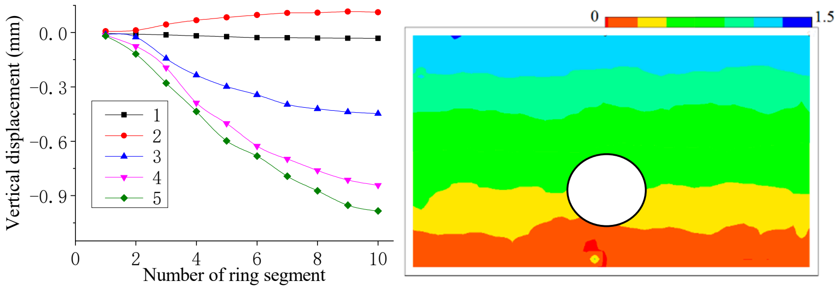


(**a**)

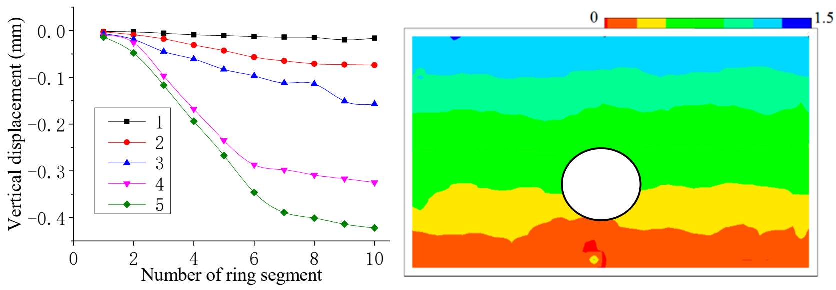


(**b**)

**Figure 14.** *Cont.*

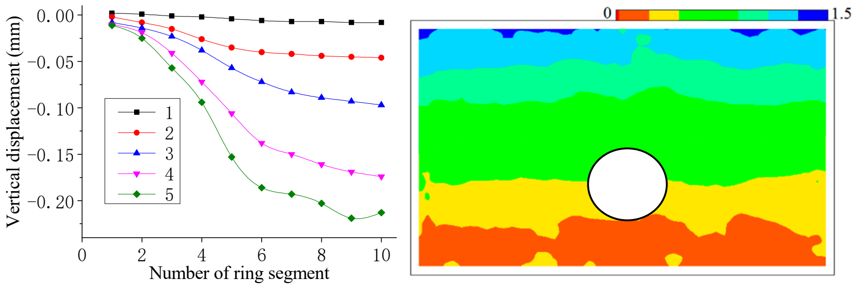


(**c**)

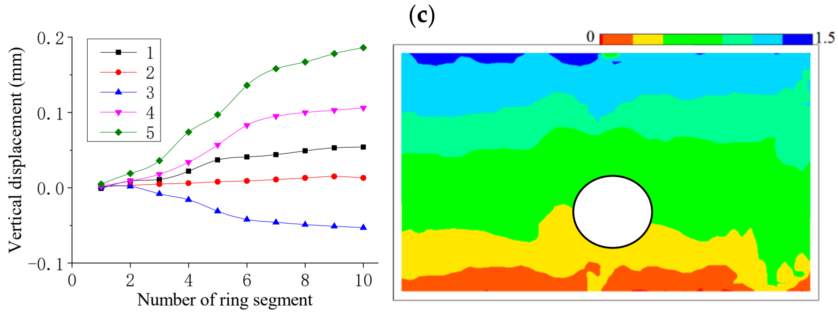


(**d**)

**Figure 14.** Displacement and contour of measuring point during shield tunneling: (**a**) Grouting filling coefficient 1.2; (**b**) Grouting filling coefficient 1.4; (**c**) Grouting filling coefficient 1.6; (**d**) Grouting filling coefficient 1.8.

When the grouting filling coefficient was 2.0, surface slurry leakage occurred; the process is shown in Figure 15. At first, the grout around the grouting hole diffused unevenly (the infiltration trend was obvious); Then, the two grouting hole diffusion rings were combined; Finally, the slurry penetrated the soil layers between the grouting holes, raising the soil layers as a whole, and the slurry lifted up vertically at the weak position.

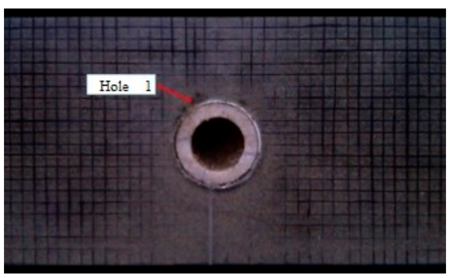


(**a**)

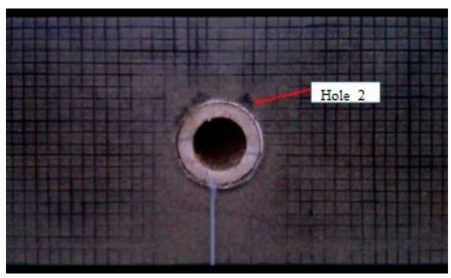


(**b**)

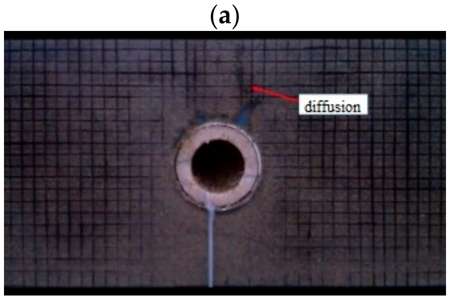


(**c**)

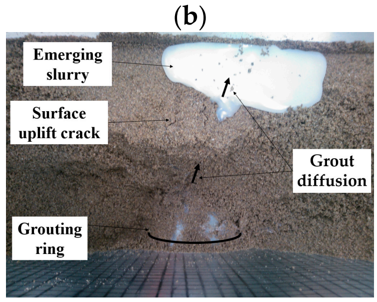


(**d**)

**Figure 15.** Grout flowing when grouting filling coefficient 2.0: (**a**) 1 hole; (**b**) 2 holes; (**c**) Grout diffusion; (**d**) Surface diffusion.

Generally, the subway construction settlement should be controlled within 30 mm. The test settlement value should be controlled within 0.3 mm according to the test similar scale of 1:100. The surface heave displacement with different grouting filling coefficients is shown in Figure 16, where the grouting filling coefficient was 1.4~1.6, and the surface displacement was relatively uniform, meeting the control conditions.

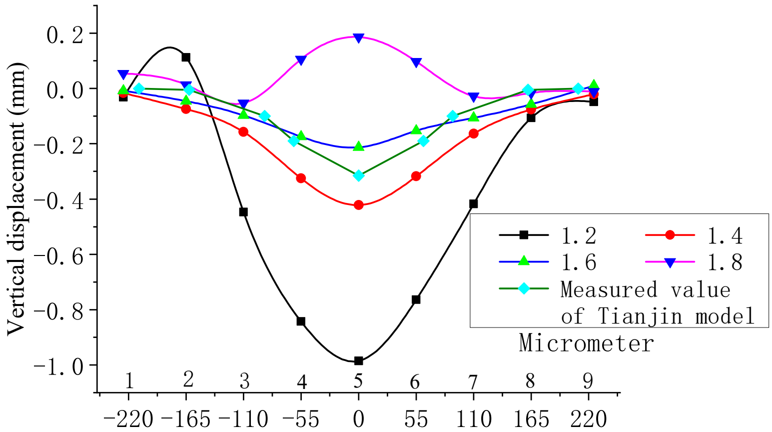


**Figure 16.** Surface displacement with different grouting filling coefficient.

The influence of different filling factors on the vertical and horizontal displacement of piles is shown in Figure 17. The displacement of piles decreases with the increase in filling factor overall. The displacement of piles is sensitive to the filling coefficient in the range of 1.4~1.6. The horizontal displacement appeared to reverse increase in the range of 1.6~1.7 and upwarping deformation appeared.

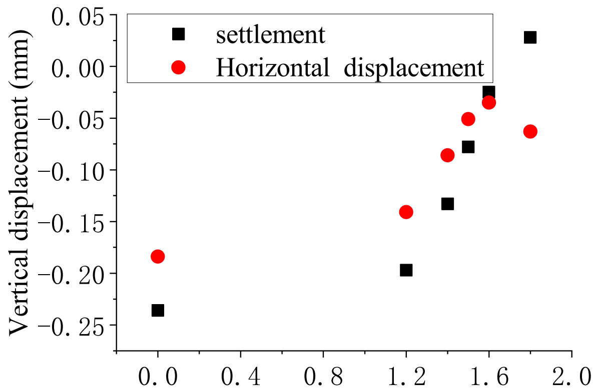


**Figure 17.** Relationship between pile displacement and grouting.

Based on the observed surface settlement and pile displacement, the recommended range of grouting filling coefficient in the silty clay layer was 1.4~1.6. The grouting filling coefficient of the gravel stratum test was given as 1.7~2.0 [7], and the grouting filling coefficient of the Shanghai shield project through muddy clay [8] was determined to be greater than 1.32. By comparing and analyzing the parameters obtained from relevant engineering cases, it could be concluded that the range of grouting filling coefficient given by this test relatively fluctuated near the above range.

When the grouting filling coefficient was 1.5, according to the analysis of the influence of pile and grouting on surface settlement in Figure 18, the grouting settlement was reduced by 77.4% compared with the no-grouting case, and the maximum settlement with pile was reduced by 19.7%, on average, compared to the no-pile case; The control effect of grouting on surface settlement was remarkable: settlement steps were generated around the pile, the loss of soil mass on the side of the pile near the tunnel was reduced effectively, and the retaining effect was obvious. The solid black straight line in Figure 18 indicates the position of the pile, which indicates the relative relationship between the ground settlement and the position of the pile.

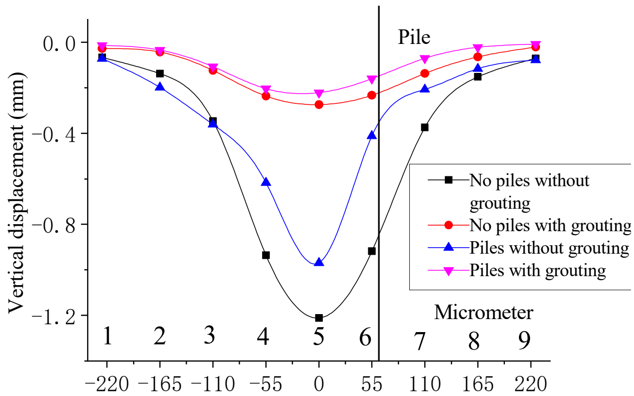


**Figure 18.** Influence of pile and grouting on the surface subsidence.

The maximum sedimentation values measured by dial gauge for the 33 sets of orthogonal tests are shown in Table 7. The reduction ratio of the maximum surface settlement of different pile positions relative to the no-pile case is shown in Table 8.

**Table 7.** The maximum settlement (mm).

| Cover Span Ratio | Lining Grouting Support | | Horizontal Position | Vertical Position | | |
|---|---|---|---|---|---|---|
| | NO | Yes | | $V = 0.5D$ | $V = 0D$ | $V = -0.5D$ |
| $H/D = 1$ | / | 0.274 | W = 1$D$<br>W = 2$D$<br>W = 3$D$ | 0.271<br>0.267<br>0.272 | 0.262<br>0.243<br>0.273 | 0.221<br>0.218<br>0.27 |
| $H/D = 2$ | 5.08 | 0.18 | W = 1$D$<br>W = 2$D$<br>W = 3$D$ | 0.178<br>0.162<br>0.172 | 0.164<br>0.154<br>0.167 | 0.144<br>0.139<br>0.166 |
| $H/D = 3$ | 4.55 | 0.12 | W = 1$D$<br>W = 2$D$<br>W = 3$D$ | 0.112<br>0.114<br>0.119 | 0.103<br>0.104<br>0.118 | 0.097<br>0.101<br>0.118 |

**Table 8.** The reduction percent of maximum settlement with different pile position (%).

| Cover Span Ratio | Horizontal Position | Vertical Position | | |
|---|---|---|---|---|
| | | $V = 0.5D$ | $V = 0D$ | $V = -0.5D$ |
| $H/D = 1$ | W = 1$D$<br>W = 2$D$<br>W = 3$D$ | 1.09<br>2.55<br>0.71 | 4.38<br>11.31<br>0.36 | 19.34<br>20.44<br>1.46 |
| $H/D = 2$ | W = 1$D$<br>W = 2$D$<br>W = 3$D$ | 1.11<br>10.00<br>4.44 | 8.89<br>14.44<br>7.22 | 20.00<br>22.78<br>7.78 |
| $H/D = 3$ | W = 1$D$<br>W = 2$D$<br>W = 3$D$ | 6.67<br>5.00<br>0.83 | 14.17<br>13.33<br>1.67 | 19.17<br>15.83<br>1.67 |

The tests showed that grouting has obvious control effects on surface subsidence, and the control degree of maximum surface settlement varies greatly with the different pile positions. The appropriate control range was 1$D$~2$D$. The surface settlement could not be well controlled if the transverse spacing between piles and tunnels was too large or too small. When the pile bottom level was below the tunnel arch waist, the control effects of ground settlement was significantly enhanced, so the driving of isolation piles should be located within the range of 1$D$~2$D$ of the tunnel, and the best effect should be achieved by further extending the pile bottom below the inverted arch.

According to the settlement data obtained under the various working conditions, the settlement curve was fitted to obtain the reverse bending point distance *i*. The linear function correction method was used to solve the settlement tank correction parameter *k* of Peck curve. The formula for fitting the relationship between *K* value and coverage-span ratio of no-piles was as follows. Table 9 shows the *K* value under the various working conditions with piles.

$$K = 1.2 - \frac{0.2H}{D} \tag{9}$$

**Table 9.** Correction coefficient of settlement trough under all working conditions.

| Cover Span Ratio | Lining Grouting Support | | Horizontal Position | Vertical Position | | |
|---|---|---|---|---|---|---|
| | NO | Yes | | $V = 0.5D$ | $V = 0D$ | $V = -0.5D$ |
| $H/D = 1$ | / | 1.006 | W = 1$D$ | 0.951 | 0.928 | 0.878 |
| | | | W = 2$D$ | 0.946 | 0.930 | 0.898 |
| | | | W = 3$D$ | 0.990 | 0.954 | 0.888 |
| $H/D = 2$ | 0.766 | 0.785 | W = 1$D$ | 0.670 | 0.640 | 0.589 |
| | | | W = 2$D$ | 0.665 | 0.618 | 0.583 |
| | | | W = 3$D$ | 0.709 | 0.692 | 0.654 |
| $H/D = 3$ | 0.482 | 0.602 | W = 1$D$ | 0.611 | 0.598 | 0.562 |
| | | | W = 2$D$ | 0.653 | 0.634 | 0.616 |
| | | | W = 3$D$ | 0.573 | 0.559 | 0.531 |

The test showed that the main influence indicators of *K* value include coverage-span ratio, soil properties, construction methods, etc. The *K* value range of clay was obtained from 0.4 to 0.6 [12]. The *K* value range of sandy soil was obtained from 0.25 to 0.45 by [13]. The *K* value range of station construction obtained by [14] the "PBA" drift-pile method from 0.61 to 0.82, and the *K* value range of the center drift excavation method was from 0.40 to 0.65 according to the specific project. The important influencing factor of *K* value obtained in this test was the coverage-span ratio. Based on the data of various working conditions, the recommended reference range of *K* value of settlement trough according to the width correction parameter can be given as:

$$\begin{cases} H/D < 0.5;\ 1.1 < K < 1.2 \\ 0.5 < H/D < 1;\ 1.0 < K < 1.1 \\ 1 < H/D < 2;\ 0.4 < K < 0.8 \\ 2 < H/D < 3;\ 0.5 < K < 0.75 \\ H/D > 3;\ K < 0.5 \end{cases} \tag{10}$$

The *K* value decreased with the increase in coverage span ratio. The *K* value of surrounding rock with piles decreased by 0.075, on average, compared with the no-piles case. The *K* value increased with the increase in pile-tunnel distance and decreased with the increase in pile burial depth.

### *4.3. Earth Pressure*

The earth pressure value caused by shield excavation was different under the different soil-pile positions. The change value of earth pressure at each position in the model test could be monitored through the micro pressure cell of No. 1–8. The radial pressure values of surrounding soil caused by shield tunneling at the different pile-tunnel locations under the working conditions of $H/D$ = 1, 2 and 3 are shown in Figures 19–21.

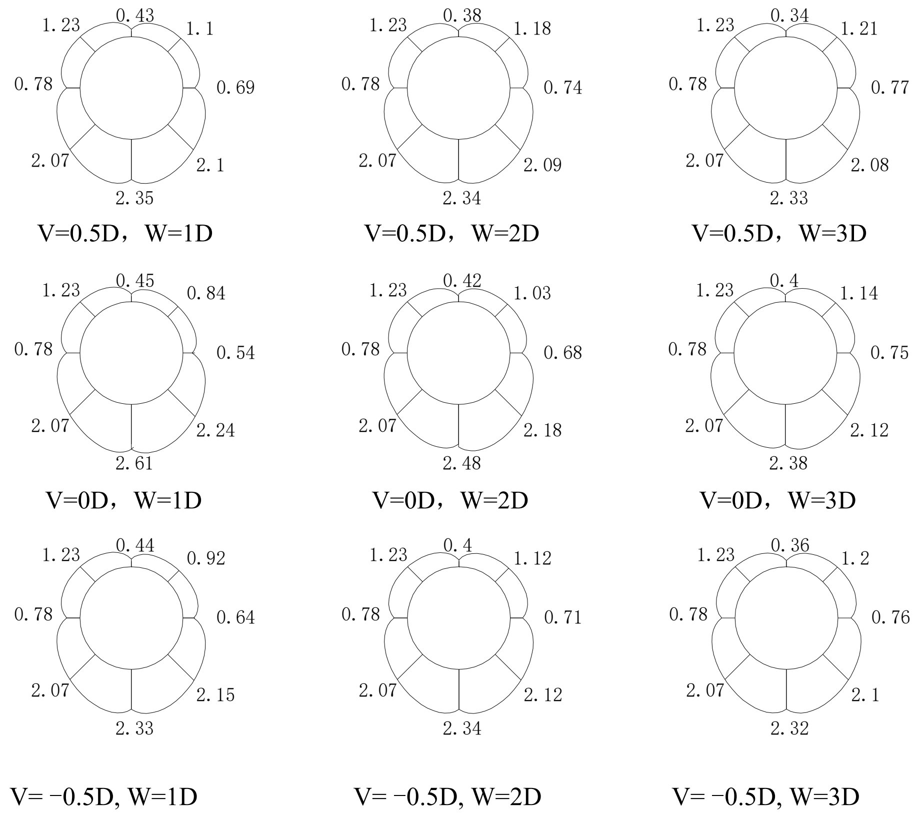


**Figure 19.** The soil pressure at different position of piles when $H/D$ = 1.

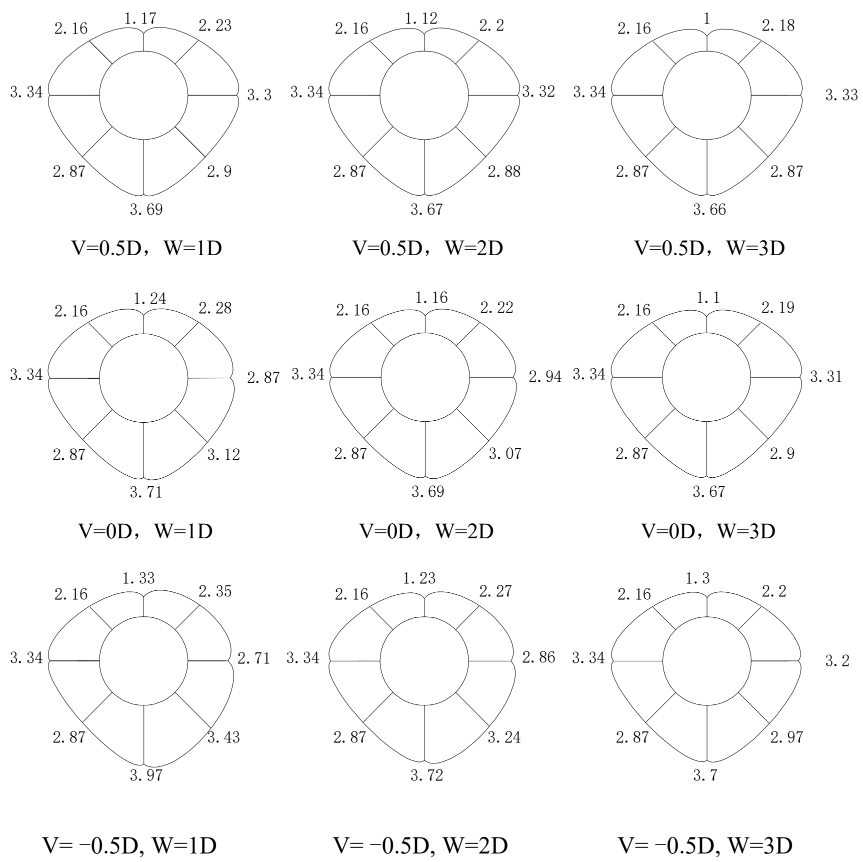


**Figure 20.** The soil pressure at different position of piles when $H/D$ = 2.

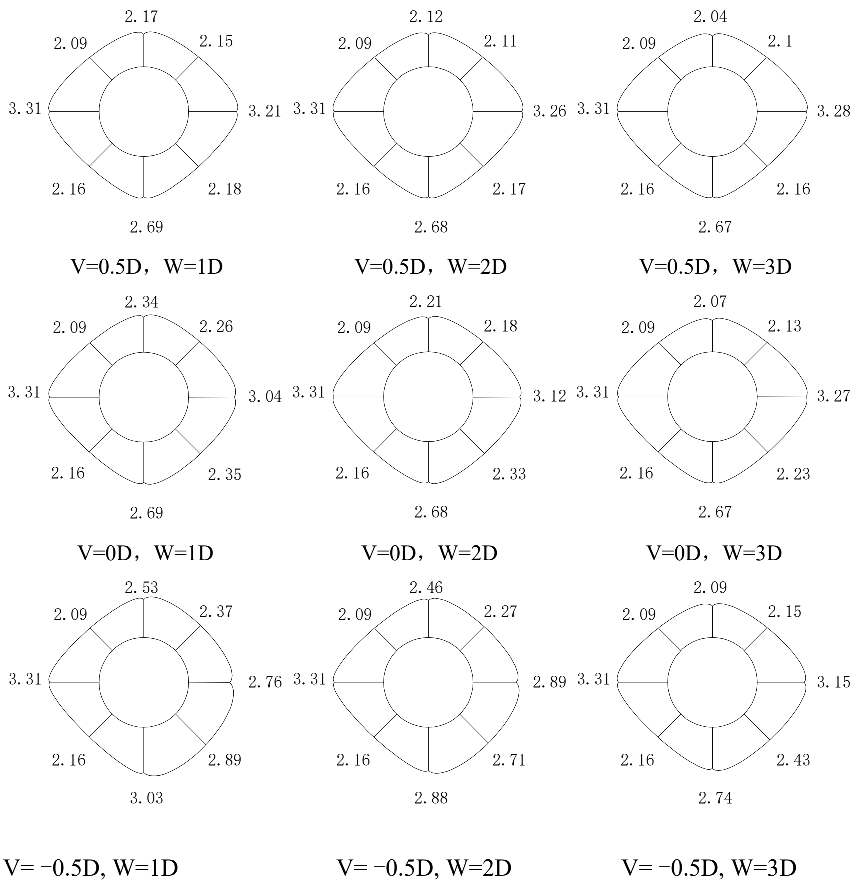


**Figure 21.** The soil pressure at different position of piles when $H/D = 3$.

The final state values of the radial earth pressure in the tunnel monitored by the orthogonal test of 27 groups showed that:

(1) With the increase in $H/D$, the earth pressure increases, and the earth pressure around the tunnel tends to be uniform. When the pile exists, the earth pressure around the tunnel present an asymmetric distribution;

(2) The existence of the pile increases the radial pressure of the nearby soil mass. When the transverse distance of the pile-tunnel was 3*D*, the influence on the earth pressure cell was small. The vertical influence range of the pile was 1 time the diameter of the pile from the bottom of the pile. When the pile bottom was located at the horizontal plane of the tunnel arch bottom, the influence on the earth pressure of the surrounding rock on the side of the pile was larger than the side of no-pile.

### 4.4. Pile Response

When the coverage-span ratio $H/D$ was 1, 2, 3, the bending moment of pile with the different pile-tunnel relative position is shown in Figures 22–24. The reduction ratio in the bending moment of the pile caused by the lateral and vertical transformation of the pile position is shown in Table 10.

**Table 10.** The reduction percent of bending moment at different position of pile (%).

| ***H/D*** | **Horizontal** | | **Vertical** | |
|---|---|---|---|---|
| | **1*D*→2*D*** | **1*D*→3*D*** | **−0.5*D*→0*D*** | **−0.5*D*→0.5*D*** |
| 1 | 65.68 | 90.54 | 57.09 | 80.61 |
| 2 | 59.23 | 84.11 | 60.28 | 53.29 |
| 3 | 60.01 | 83.94 | 39.49 | 67.54 |

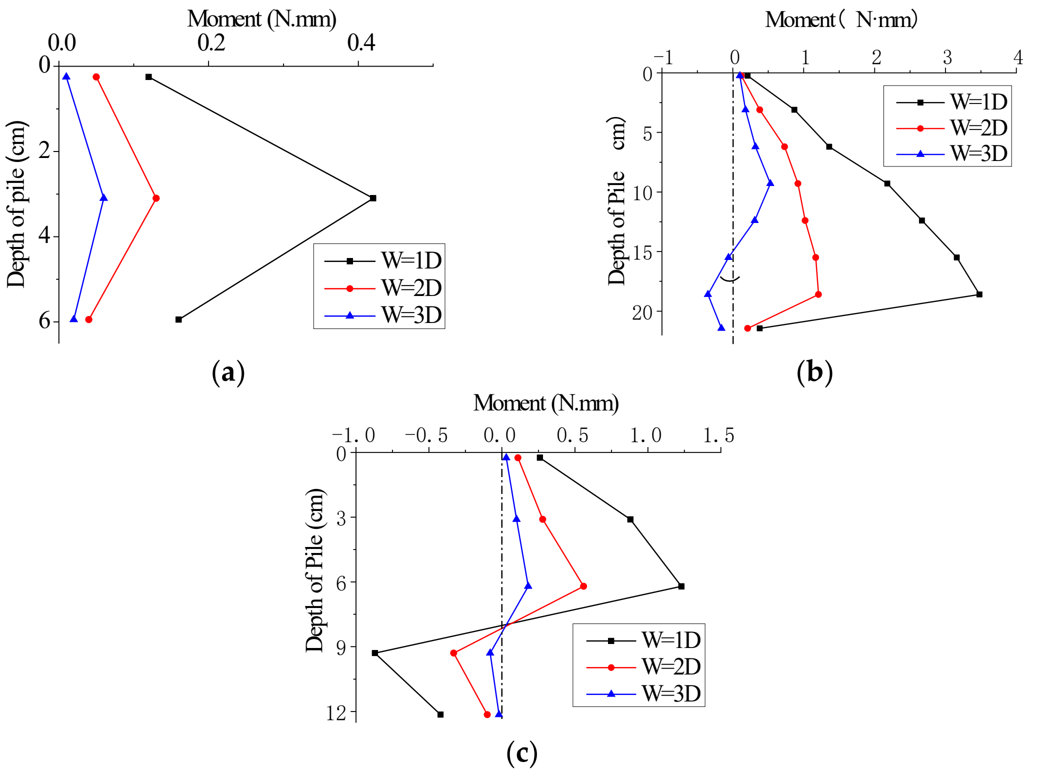


**Figure 22.** Bending moment of pile at different vertical positions when $H/D = 1$: (**a**) $V = 0.5D$; (**b**) $V = 0D$; (**c**) $V = -0.5D$.

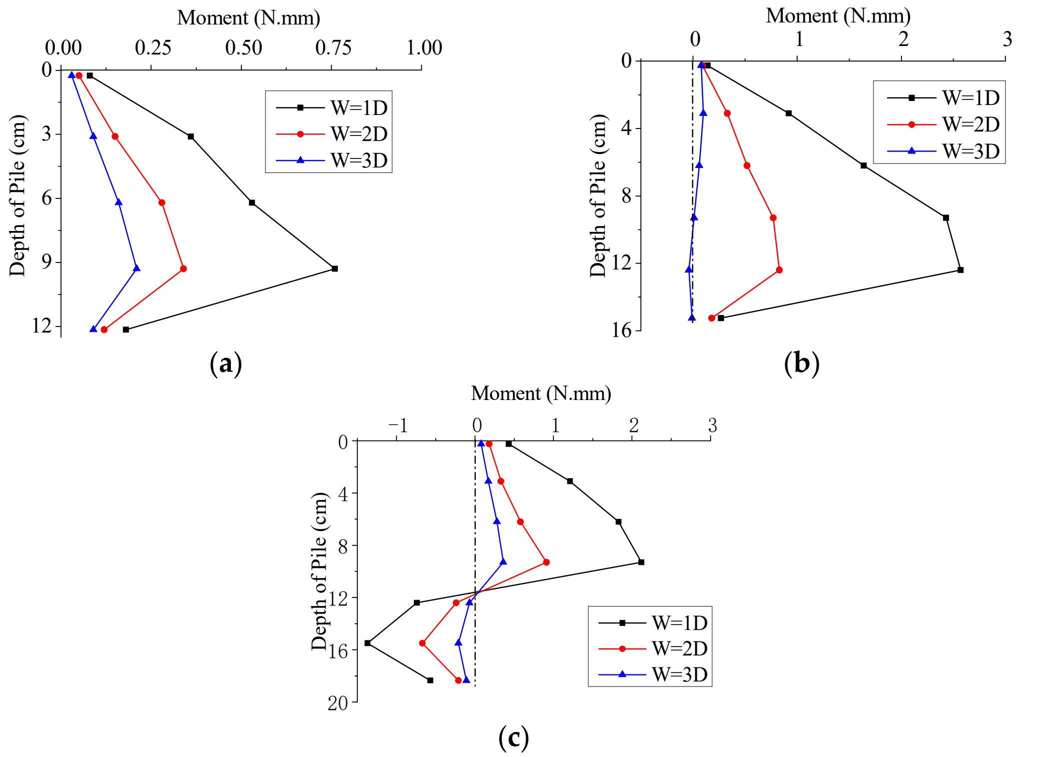


**Figure 23.** Bending moment of pile at different vertical positions when $H/D = 2$: (**a**) $V = 0.5D$; (**b**) $V = 0D$; (**c**) $V = -0.5D$.

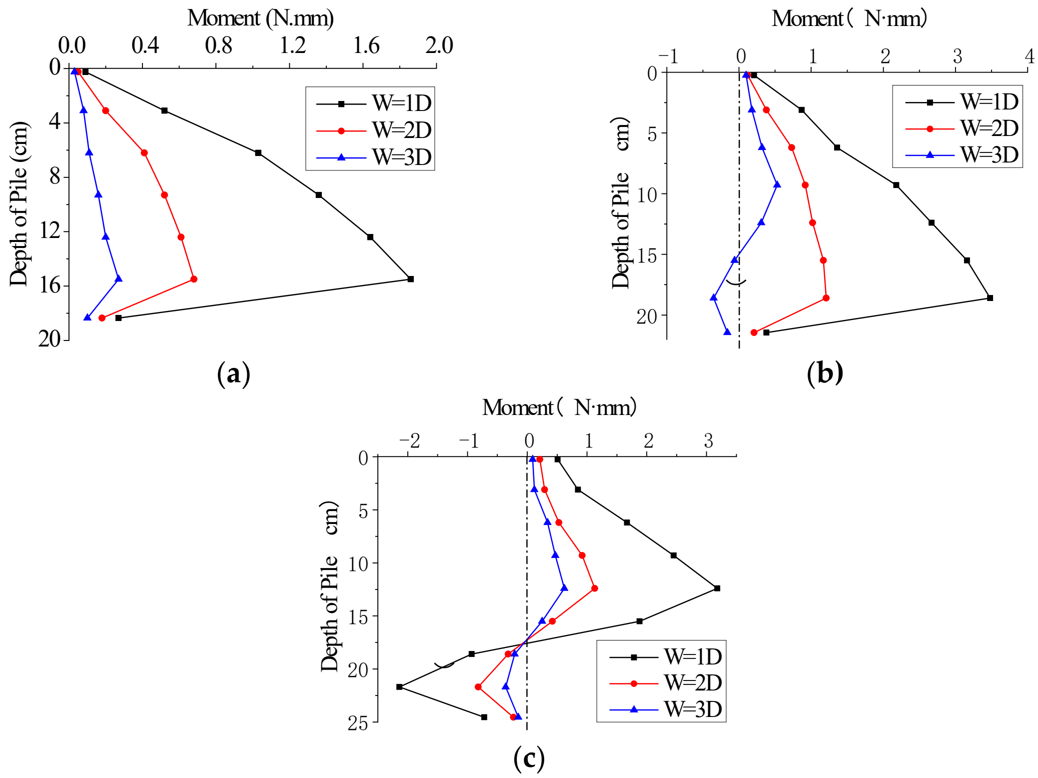


**Figure 24.** Bending moment of pile at different vertical positions when $H/D = 3$: (**a**) $V = 0.5D$; (**b**) $V = 0D$; (**c**) $V = -0.5D$.

The following conclusions and rules were obtained from the above tests:

(1) The greater the coverage span ratio was, the bending moment of the pile at the same level was larger; when the pile bottom was located at or above the tunnel chamber line, the maximum bending moment was generally located at the middle or lower part of the pile. When the pile bottom was located below the tunnel chamber line, the pile appeared at the negative bending moment, and the maximum negative bending moment was located at the arch waist.

(2) The bending moment value change was obvious due to the influence of the lateral position change for the pile-tunnel system. The maximum influence area was $1D \rightarrow 2D$, and the influence degree outside $2D$ was significantly weakened. The change in vertical position has a great influence on the direction of the bending moment. The maximum influence range was that the pile bottom located in the range from the arch waist (v = 0d) to the arch bottom (v = −0.5d), and the bending moment from the arch waist (v = 0d) to the arch crown (v = 0.5d) was similar and affected much by the buried depth. The larger the cover-span ratio $H/D$ was, the weaker the influence of tunnel excavation on piles would be.

When the coverage-span ratio $H/D$ was 1, 2 and 3, the vertical settlement of piles at different relative positions of pile-tunnels was shown in Figure 25. The reduction ratio of pile settlement due to the lateral and vertical transformation of the pile position is shown in Table 11.

**Table 11.** The reduction percentage of settlement at different position of pile (%).

| ***H/D*** | **Horizontal** | | **Vertical** | |
|---|---|---|---|---|
| | **1*D*→2*D*** | **1*D*→3*D*** | **0.5*D*→0*D*** | **−0.5*D*→0.5*D*** |
| 1 | 41.44 | 63.63 | 8.33 | 19.54 |
| 2 | 56.11 | 65.69 | 9.27 | 19.28 |
| 3 | 61.41 | 72.56 | 7.42 | 13.69 |

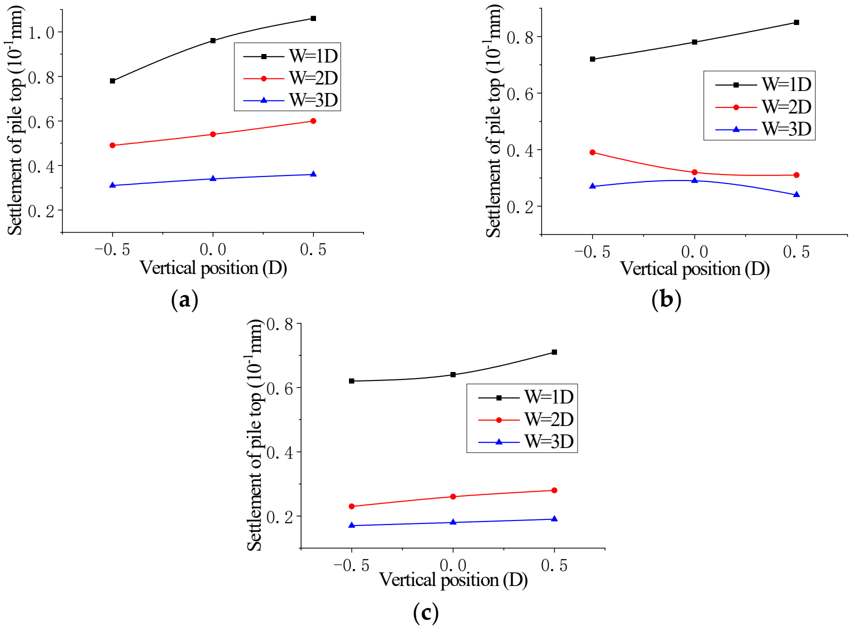


**Figure 25.** Settlement of pile top: (**a**) $H/D$ = 1; (**b**) $H/D$ = 2; (**c**) $H/D$ = 3.

From the above test data, it could be seen that the larger the coverage-span ratio was, the smaller the pile settlement was. The lateral position change in the pile-tunnel had a great impact on the settlement. The $1D \rightarrow 2D$ settlement decreased greatly, with an average reduction of 52.99%, and the $2D \rightarrow 3D$ settlement reduced, on average, by 14.31%. When the pile bottom was vertically located at the horizontal line of the arch crown ($V$ = 0.5$D$), the settlement was the largest. When the pile bottom was below the arch waist, the vertical settlement was controlled to a certain extent. The greater the buried depth of the pile, the smaller the vertical settlement value was.

When the coverage span ratio $H/D$ was 1, 2 and 3, the horizontal displacement of piles at different relative positions of pile-tunnels is shown in Figure 26. The reduction ratio of the horizontal displacement of the pile caused by the horizontal and vertical transformation of the pile position is shown in Table 12.

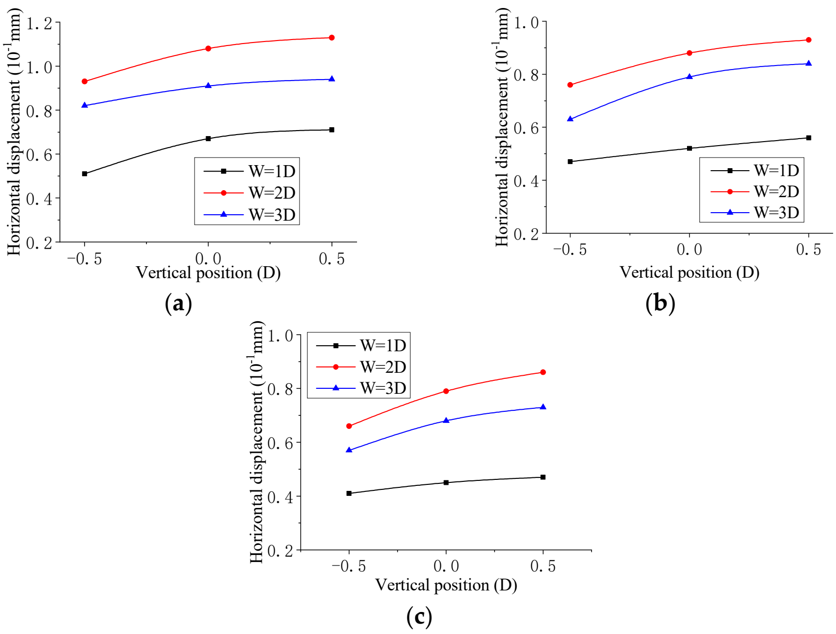


**Figure 26.** Horizontal displacement of pile top: (**a**) $H/D$ = 1; (**b**) $H/D$ = 2; (**c**) $H/D$ = 3.

**Table 12.** The reduction percent of horizontal displacement at different position of pile (%).

| *H/D* | Horizontal | | Vertical | |
|---|---|---|---|---|
| | **2*D*→1*D*** | **2*D*→3*D*** | **0.5*D*→0*D*** | **−0.5*D*→0.5*D*** |
| 1 | 40.10 | 14.79 | 4.41 | 19.55 |
| 2 | 39.62 | 12.34 | 6.16 | 19.78 |
| 3 | 42.09 | 14.23 | 6.42 | 19.32 |

It can be seen from the variation law of the horizontal displacement of piles at different pile positions caused by shielding that the larger the coverage-span ratio was, the smaller the horizontal displacement was, and the influence of the lateral distance between the pile-tunnel was greater. The horizontal displacement was larger when it was twice the tunnel diameter (W = 2*D*) from the tunnel axis, which indicated that the influence range of grouting around the pile was about 2*D*. The horizontal displacement decreased by 40.60%, on average, from the 1*D*→2*D*, and decreased by13.79%, on average, from the 2*D*→3*D*. The influence of the vertical position change in the pile on the horizontal displacement was not related to $H/D$, but still showed that when the pile bottom was located in the horizontal line of the arch bottom (V = − 0.5*D*), the horizontal displacement of the pile was well controlled.

Due to the existence of the size effect of the model experiment, a prediction of the prototype is limited only to the model study results; the model experiment results and the finite element 1:1 model analysis results were compared in the paper and the results were relatively matched. The predictions made by the prototype test are relatively credible and a follow-up with similar experiments with enlarged scales could be conducted to carry out comparative analysis considering the size effect.

### *4.5. Model of the Zonal Blockization of Surrounding Rock*

Combined with the influence of shielding on the deformation and stress field of the weak surrounding rock, the bending moment and displacement of the adjacent pile were analyzed. The zonal block model of the shallow tunnel surrounding rock had a regional division, which is shown in Figure 27.

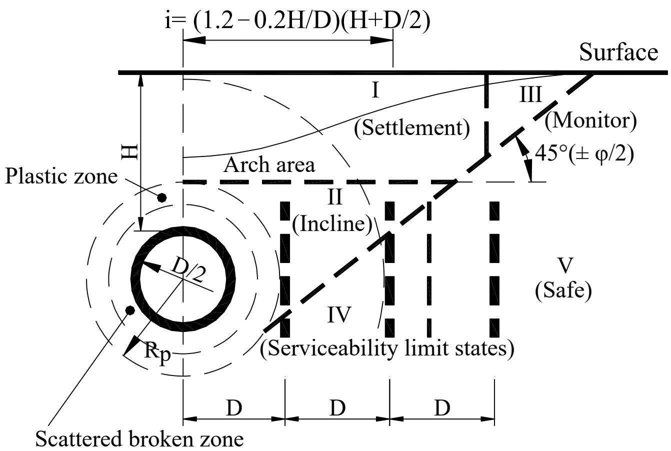


**Figure 27.** Region division of rock with pile when shield.

The weak surrounding area around the pile side was divided into five parts: the coordinated movement of surrounding rock and pile in zone I was the most intense, with the largest settlement and horizontal displacement. Safety construction measures such as reinforcement and underpinning piles to prevent over-settlement of buildings and structures in this area should be taken. It is recommended that the short piles in this area should be densely distributed. Zone III will be affected by shielding construction, but generally it would not pose a great threat to the normal use and the safety of buildings and structures. Real-time monitoring should be carried out during construction. If piles were driven in this area, it is recommended to use sparse piles and keep them deeply buried. engineering accidents such as pile over-displacement or inclination are expected. When the shield jacking force acts on the tunnel face, the jacking can easily cause the pile to bend back or forth along the jacking direction, and the pressure change in shield tail grouting can cause the pile to bend left or right perpendicular to the tunnel axis. In the actual shield construction process, isolation and reinforcement measurements should be constructed to prevent the pile from excessive settlement and inclination and prevent the internal force and deformation of the pile from reaching a limited state. The settlement of piles in Zone IV was small, but due to the stress release of surrounding rock near the arched camber line, the piles bear negative bending moments. The uneven stress effect of the piles would pose a threat due to different shield friction and grouting parameters at the same time. The main factors considered in this area were the limit state of the normal use of piles and the according safety issues. This area could be considered the best zone for an isolation pile driving area. Zone V could be considered as the safe area for the pile-shielding system. Shield excavation has little impact on these surrounding layers, which neither cause the large displacement nor the ultimate bending moment of the pile.

Similar conclusions or laws can be compared according to the references [15–18].

## 5. Conclusions

A series of model tests was conducted on the shield-tunnel adjacent to the pile system in the silty clay layer of a coastal area. The response of weak surrounding layers and adjacent piles caused by shield tunneling were observed.

Similar problems were found in the modeling experiment of the equivalent materials for lining, including weak surrounding rock, similar materials of piles, and developed functions of automatic jacking and synchronous grouting at the tail of shield.

In total, 33 groups of orthogonal models were independently designed to study the progressive failure caused by tunnel excavation in the silty clay layers, The following issues of stratum displacement, the displacement and internal force response of piles and earth pressure change were also considered.

The following conclusions can be drawn:

(1) The best grouting filling coefficient for the shielding case was 1.4~1.6;
(2) The suggested range of settlement trough width parameters were obtained by fitting the experimental data. The $K$ value of pile-surrounding layers with piles was reduced by 0.075, on average, compared with that of the no-piles case. The $K$ value increased with the increase in pile-tunnel distance and decreased with the increase in pile burial depth in the research example.
(3) A model of the zonal blockization of surrounding rock was given. They were divided into five reasonable zones according to the displacement, pressure change and pile response of the weak surrounding layers in the pile-tunnel system, and the characteristics of its key construction control methods were given.

**Author Contributions:** Conceptualization, X.G. and Z.L.; methodology, X.G.; software, M.P.; investigation, X.Z.; data curation, Z.L.; writing—original draft preparation, Z.L.; writing—review and editing, X.Z.; supervision, X.G. All authors have read and agreed to the published version of the manuscript.

**Funding:** This research was supported by Sichuan-Tibet special fund of the Fundamental Research Funds for the Central Universities (2022JBCZ002); Research Project of China Railway Fifth Survey and Design Institute Group: 5y2021-c29 (Beijing Jiaotong University grant number C22L00310); Research Project of China Railway Group: N2021G057 (Beijing Jiaotong University grant number C22D00020).

**Institutional Review Board Statement:** Not applicable.

**Informed Consent Statement:** Not applicable.

**Data Availability Statement:** Data are contained within this article.

**Acknowledgments:** The authors thank the reviewers for their great help on the article during the review process.

**Conflicts of Interest:** The authors declare no conflict of interest. The funders had no role in the design of the study; in the collection, analyses, or interpretation of data; in the writing of the manuscript, or in the decision to publish the results.

## References

1. Hu, X.Y.; Yan, Q.X.; He, C.; Yang, X.Y. Model test and 3D dem analysis on the failure feature of excavation face and disturbance of granular mixtures stratum due to epb shield tunneling. *Chin. J. Rock Mech. Eng.* **2016**, *35*, 1–10. (In Chinese)
2. Hergarden, H.J.A.M.; Vander Poel, J.T.; Vander Schrier, J.S. Ground movements due to tunneling: Influence on pile foundation. In Proceedings of the International Symposium on Geotechnical Aspects of Underground Construction in Soft Ground, Tokyo, Japan, 19–21 July 1996; Balkema: Rotterdam, The Netherlands, 1996; pp. 519–524.
3. Ghahremannejad, B.; Surjadinata, J.; Poon, B.; Carter, J.P. Effects of tunneling on model pile foundations. In Proceedings of the 6th International Conference on Physical Modelling in Geotechnics, Hong Kong, China, 4–6 August 2006; pp. 1157–1162.
4. Selemetas, D.; Standing, J.R.; Mair, R.J. Response of full scale piles to tunneling. In Proceedings of the 5th International Symposium on Geotechnical Aspects of Underground Construction in Soft Ground, Amsterdam, The Netherlands, 5–17 June 2005; Taylor & Francis: London, UK, 2005; pp. 763–769.
5. Bai, B.; Yang, G.C.; Li, T.; Yang, G.S. A thermodynamic constitutive model with temperature effect based on particle rearrangement for geomaterials. *Mech. Mater.* **2019**, *139*, 103180. [CrossRef]
6. Bai, B.; Xu, T.; Nie, Q.K.; Li, P. Temperature-driven migration of heavy metal Pb 2 + along with moisture movement in unsaturated soils. *Int. J. Heat Mass Transf.* **2020**, *153*, 119573. [CrossRef]
7. Yu, L.; Zhang, D.L.; Fang, Q.; Li, Y.; Wang, G.; Cao, L. Analytical Prediction of Strip Foundation Building Response to Shallow Tunneling Considering the Tunneling Process. *Appl. Sci.* **2022**, *12*, 4656. [CrossRef]
8. The Second Survey and Design Institute of China Railway. *TB10003-2005, Code for Design of Railway Tunnel*; China Railway Publishing House: Beijing, China, 2005. (In Chinese)
9. Wang, S.P. Model Test Study on the Tunnel within Cracked Surrounding Rocks. Ph.D. Thesis, Zhejiang University, Hangzhou, China, 2004. (In Chinese).
10. Yu, C.R. Research on Grouting Influence and Mechanism of Shield Tunneling in the Sand-Gravel Stratum. Ph.D. Thesis, Shanghai Jiao Tong University, Shanghai, China, 2011. (In Chinese).
11. Pan, K.; Li, M.Y.; Yuan, D.K. Analysis of the DOT tunneling construction parameters in special formation. *Strut. Eng.* **2010**, *26*, 125–129. (In Chinese)
12. O'Reilly, M.P.; Newb, M. *Settlement above Tunnels in the United Kingdom-Their Magnitude and Prediction*; The National Academies of Sciences, Engineering, and Medicine: Washington, DC, USA, 1982; pp. 173–181.
13. Yoshikoshi, W.; Watanabe, O.; Takagi, N. Prediction of ground settlements associated with shield tunneling. *Soils Found.* **1978**, *18*, 47–59. [CrossRef]
14. Wang, T.; Liu, W.N.; Zhang, C.M.; He, H.; Li, X. Study on ground settlement induced by shallow metro station construction. *Chin. J. Rock Mech. Eng.* **2007**, *26*, 1855–1861. (In Chinese)
15. Zhang, Y.; Su, G.S.; Li, Y.; Wei, M.D.; Liu, B.C. Displacement back-analysis of rock mass parameters for underground caverns using a novel intelligent optimization method. *Int. J. Geomech.* **2020**, *20*, 04020035. [CrossRef]
16. Li, Z.W.; Tao, M.; Du, K.; Cao, W.Z.; Wu, C.Q. Dynamic stress state around shallow-buried cavity under transient P wave loads in different conditions. *Tunn. Undergr. Space Tech.* **2020**, *97*, 103228. [CrossRef]
17. Li, W.; Zhang, C.P. Face stability analysis for a shield tunnel in anisotropic sands. *Int. J. Geomech.* **2020**, *20*, 04020043. [CrossRef]
18. Chen, G.H.; Zou, J.F.; Qian, Z.H. An improved collapse analysis mechanism for the face stability of shield tunnel in layered soils. *Geomech. Eng.* **2019**, *17*, 97–107.